Effects of geometry in pressure–shear and normal plate impact recovery experiments: Three-dimensional finite-element simulation and experimental observation

Ashok R. Machcha and Sia Nemat-Nasser
Center of Excellence for Advanced Materials, Department of Applied Mechanics and Engineering Sciences, University of California, San Diego, La Jolla, California 92093

(Received 9 May 1995; accepted for publication 23 May 1996)

The minimization of the radial release effects in the recovery configurations of plate impact experiments is essential for accurate postmortem microstructural investigations. The present study evaluates the results of several three-dimensional finite-element simulations involving different plate geometries. The study examines combinations of circular, square, and star-shaped plate geometries, with no lateral momentum traps or guard rings. Experiments and simulations are conducted on brittle specimens. A simple, but fairly successful, combination for the pressure–shear recovery experiment is reported, which makes use of a single square and three circular plates. In the case of the normal impact recovery configuration, it is found that the star-shaped flyer in combination with the square target and momentum trap gives good results at locations away from the axis of the specimen. Crack patterns observed experimentally in the conventional nonrecovery pressure–shear mode, and in recovery pressure–shear and normal impact modes are discussed in relation to the simulation results. © *1996 American Institute of Physics.* [S0021-8979(96)04617-8]

I. INTRODUCTION

Plate impact experiments are used to study dynamic deformation and failure modes of materials at high strain rates. The recovery configurations in these experiments are performed with the objective of examining the microstructural changes in the specimen after it is subjected to loading under a uniaxial strain condition. The experiments are designed to achieve a controlled plane–wave loading of the specimens. In practice, this is limited by the finite size of the plates employed, which generate radial release waves. This has the potential for significant contribution to the damage processes by introducing causes other than the uniaxial straining of the material. Hence, this aspect of the plate impact experiment has been the subject of considerable research in the past.

A plate impact experiment involves the impact of a moving flat plate, called a flyer, with another stationary plate, called the target, which is usually the specimen. In the normal plate impact experiment, the specimen is subjected to a compression pulse. The material at the center of the specimen then is under a uniaxial strain condition. In the pressure–shear experiment the specimen undergoes a combined compression and shearing. Thus, the material undergoes a transverse shearing while it is in a compressed condition. The wave propagation is one dimensional, since both the pressure and shear pulses travel along the same axis. The recovery configuration in the normal impact mode employs a backing plate for the target, to capture the longitudinal momentum. In the pressure–shear recovery mode,[1] two flyer plates, which are separated by a thin lubricant layer, are used along with the backing plate to capture the longitudinal and shear momenta. The amount of the trapped shear momentum depends on the shear strength of the lubricant. The impedances of all the plates have to be reasonably matched, to obtain good results. Figure 1 shows the time–distance diagrams for the recovery experiments and Fig. 2 shows the experimental layout for a typical pressure–shear recovery experiment.

One of the earliest efforts to decrease the release wave effects was by Smith[2] and Hartman,[3] who used guard rings around the circumference of the sample. A similar approach was followed more recently by Chang *et al.*[4,5] who used side momentum traps. Others have used confining fixtures that encapsulate the specimens, such as Louro and Meyers.[6] This approach has the disadvantage of the need for close tolerances in machining, making the specimen preparation and assembly difficult. A different approach was followed by Kumar and Clifton,[7] who made use of a star geometry for the flyer to redirect the release waves and decrease their damaging effect at the center. This was implemented in experimental studies by a number of researchers.[5,8–12] Three-dimensional simulations on different configurations have been conducted by Stevens and Jones,[13] Rabie, Vorthman, and Dienes,[14] Kirkpatrick *et al.*,[15] Chang *et al.*,[5] and Espinosa *et al.*[12] All the above investigations have been for the normal impact configuration, which led to several recommendations for this configuration. Experimental evidence shows that it is difficult to recover brittle specimens intact, even at moderate stresses of about 2.0 GPa. Results from numerical simulations, gathered so far, suggest that thin flyer plates must be used, which lead to short loading durations. This is difficult to implement in the pressure–shear recovery scenario, due to practical constraints, since it requires very thin plates resulting in a negligible shear pulse duration. Hence, there is a need to consider situations involving relatively long duration pulses in pressure–shear recovery experiments. No published simulation studied of pressure–shear experiments seem to exist in the literature.

The objective of the present study[16] is to investigate the release effects, mainly in the pressure–shear recovery experiments conducted on brittle materials. The normal recov-

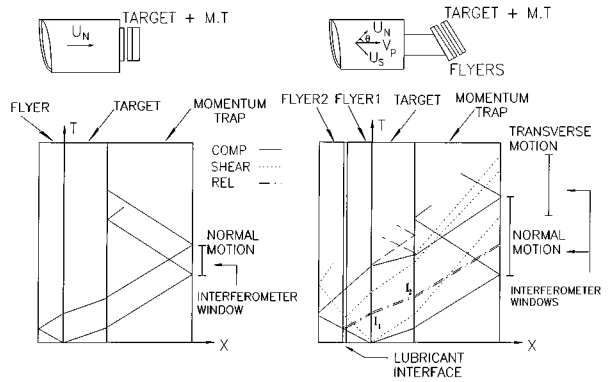

FIG. 1. Time–distance diagrams for normal and pressure–shear recovery configurations.

ery configuration is also examined for comparison purposes. This study is based on the philosophy of using the geometry of the plates to mitigate release effects and to check if a better performance is possible when a controlled breakup of the specimen is effected. In the pressure–shear configuration, some fraction of the energy is present as shear momentum. The effect of this additional momentum component on the radial release wave, before it is trapped, needs to be investigated. The question of the residual shear pulse, which arises because of the shear strength of the lubricant, is not addressed in this work.

With the above factors in mind, three-dimensional finite-element simulations are conducted, where different combinations of geometries, i.e., circular, square, and two types of star shapes are employed for the plates. Most of the simulations are performed for the circular specimen plates, since this is commercially the most easily available geometry for specimen materials. The results are discussed in relation to the experimental observations on aluminum oxide.

II. SIMULATION

The numerical simulations are carried out using DYNA-3D,[17] which was developed at the Lawrence Livermore

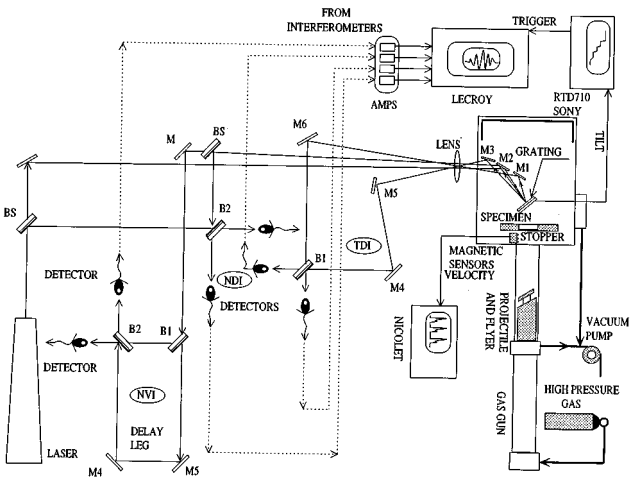

FIG. 2. Layout of a pressure–shear recovery experiment.

TABLE I. Material properties.

Material	Young's modulus (GPa)	Density (kg/m^3)	Poisson's ratio	Wave speeds (mm/μs)	
				Longitudinal	Transverse
AD99.5	372	3890	0.22	10.44	6.25
Maraging steel	200	7805	0.29	5.797	3.15

National Laboratory. This is an explicit, nonlinear, three-dimensional finite-element code for analysis of large-deformation dynamic problems. The material in the present study is an aluminum oxide ceramic (AD 99.5). The flyer and momentum trap are made of maraging steel. The difference in the longitudinal impedances of these two materials is about 10%. Their properties are given in Table I. The specimen is a very brittle ceramic. It is considered to be homogeneous and isotropic. Hence, the analysis is based on a linearly elastic material model. The simulations are conducted for three different configurations, i.e., basic pressure–shear (nonrecovery), normal recovery, and pressure–shear recovery. The circular plates used are 38.1 mm in diameter, while the square plates in the pressure–shear recovery experiments are 25.4 mm on the side. All the thicknesses and the number of elements used in the thickness direction are maintained the same for each configuration to ensure consistency. Eight-node hexahedron elements are used for the finite-element discretization. The details of the discretization are given in Tables II and III.

The interfaces between the flyer, specimen, and momentum trap are simulated as sliding surfaces which allow friction and separation. A friction coefficient of 0.35 is used for the pressure–shear experiments, since the surfaces are roughened. A value of 0.3 is used for the normal recovery experiments. The flyer–flyer interface in the pressure–shear recovery experiment is considered to be an ideal frictionless one, because of the presence of the lubricant. Initial velocity conditions are imposed on all the plates. The flyers are given velocities of 100 m/s in the normal direction (the z axis) in all simulations. In addition to this, a transverse velocity of 25 m/s (the positive x axis) is given to the flyers in the pressure–shear experiments. The specimen and momentum traps are considered to be at rest. Thus, there is an extra momentum input for the pressure–shear simulation, which has to be kept in perspective, while comparing the results with those of the normal configuration. Two planes of symmetry exist, for the normal recovery experiments, and hence only one-quarter of the assembly is considered for modeling. In the case of the pressure–shear experiments, a single plane of symmetry exists, and hence half of the assembly is examined.

Two types of star flyers, with external angles of $\pi/2$ and $3\pi/4$, as described by Kumar and Clifton,[7] are considered in the simulations. The first type is used in combination with square-shaped plates, and the second type is used in combination with the circular plates, similar to the configuration employed by Vorthman and Duvall[8] and Yaziv[10] for the normal impact experiments.

TABLE II. Details of plates used.

	Specimen	Mom. trap	Flyer1	Flyer2
Material used	AD99.5	Maraging steel	Maraging steel	Maraging steel
Configuration type	No. of thickness elements and ⟨thickness⟩			
Basic press–shear	15⟨3.0 mm⟩	⋯	20⟨2.0 mm⟩	⋯
Press–shear recovery	12⟨3.01 mm⟩	17⟨3.92 mm⟩	8⟨0.94 mm⟩	10⟨2.52 mm⟩
Normal recovery	15⟨2.0 mm⟩	17⟨3.0 mm⟩	13⟨2.0 mm⟩	⋯

The next simulation employs a square-shaped plate for the second flyer. This design evolved after observing the pattern of break up that was occurring in other experiments. In experiments where only circular geometries are used, the specimen breaks into small pieces, after a concentric portion of it has separated out. The separation seems to be assisted by the thin notches that are cut out in the specimen for tilt measurements; see Fig. 3.

The schematic diagram of the new design is shown in Fig. 3. A square plate of dimensions smaller than the other plates is used for the second flyer in the pressure–shear recovery experiment. When the wave reaches the rear surface of the first flyer, a square-shaped loading is maintained over the whole surface of the specimen, after the initial loading. A radial release wave is initiated from the lateral boundaries of the specimen. The square has four edges where cylindrical release waves can be generated, leading to fewer interacting waves. These interact with the radial release waves, generating tension in the specimen between its free boundary and a central square portion. Also, as a result of the redirection of these waves, the concentric focusing effect of the boundary is weakened. The square compression pulse traveling into the second flyer, unloads at its free surface and returns back to unload the specimen completely. This unloading wave interacts with the radial release wave, again leading to a tension along a central square portion of the specimen. This central square is positioned such that the shearing direction is along one of the diagonals of the square, which results in the shear being at an angle of 45° to the direction of the cylindrical release wave front from the square edges. Thus, the new design allows using readily available circular specimens in a configuration which redirects the focusing effect from the boundaries,[13] providing for a controlled lateral breakup of the sample. This also leads to an expenditure of the destructive radial release energy.

Since the breakup is expected to play an important role in improving performance, it was sought to simulate the involved process. Two simulations are conducted to investigate the above-mentioned configuration. One provides for the possibility of a breakup while the other does not. DYNA-3D has the capability to separate planes at a given critical strength. This capability is used to simulate a controlled breakup of the specimen, by specifying planes that could fail under tension or shear. The planes chosen for this purpose form the square shape that is observed in experiments. A tensile and shear strength of 0.4 GPa is prescribed for these planes. The location of the planes specified is based on the experimental results. No symmetry plane is used for this simulation.

The idea of employing a combination of three flyer plates, i.e., a circular plate backed by a square, which in turn is backed by a star-shaped plate, was also considered, but it was decided that equivalent simulation results are obtained from investigations involving three square plates and a star-shaped flyer.

The last simulation involves two square plates. One of the square plates is the second flyer mentioned above and the other one is the momentum trap. These two plates are positioned such that, when their flat faces are brought together,

TABLE III. Details of 3D finite-element discretization.

	No. of brick elements				
Configuration type	Total	Specimen	Mom. trap	Flyer1	Flyer2
Basic press–shear					
All cylinders	37 152	25 056	⋯	12 096	⋯
Press shear recovery					
All cylinders	37 152	9 504	13 824	6 048	7 776
One-square flyer	37 152	9 504	13 824	6 048	7 776
Separating planes	58 596	21 780	19 200	8 400	9 216
Two-square flyers	33 120	9 504	9 792	6 048	7 776
Star flyer—Π/2 type with square plates	36 720	8 800	12 800	8 064	7 056
Star flyer—3Π/4 type	36 576	9 504	13 824	6 048	7 200
Normal recovery					
All cylinders	34 560	10 752	14 592	9 216	⋯
Star flyer—Π/2 type with square plates	49 704	18 144	24 624	6 936	⋯
Square flyer	37 008	10 752	14 592	11 664	⋯

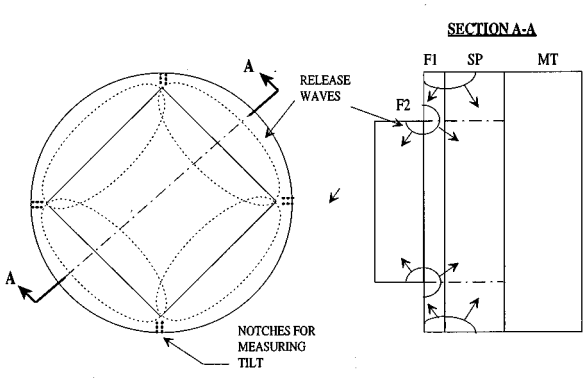

FIG. 3. New design employing a square second flyer for pressure–shear recovery configuration.

they form a star of external angle $3\pi/4$ [see Fig. 7(f)]. The idea behind this is to see if the specimen could be made to experience the effect of a star-shaped release wave near its central region through the thickness, because of the square releases on its impact and rear surfaces. The idea still needs to be fine tuned, by changing thicknesses properly, and has not been examined in sufficient detail.

In these simulations, the impact event was considered for a total duration of 5 μs for the pressure–shear configuration and 10 μs for the normal impact configurations.

III. NUMERICAL RESULTS

The results from the simulations are presented as stress, particle velocity, and pressure histories. Two locations are chosen on the specimen for obtaining results. One is at the center of the specimen and the other about 3–5 mm away. At each of these locations, three points in the thickness direction, i.e., at the impact, rear, and midsection planes, are chosen to examine the response histories. The relative starting positions on the time axis of the various plots, identify the location of the point in the thickness direction. In some plots, stress histories at only two of the positions are plotted, so that the details are not obscured. The pulses are slightly rounded and have a finite rise time due to the discretization effects. The main pulse is also broadened because of this and the reflections and reloading at interfaces, due to a mismatch of approximately 10% in the longitudinal impedances. This does not pose a problem in interpreting the time histories of the various components of the stress tensor, after long durations, i.e., by the time several wave reflections have already taken place.

In uniaxial strain conditions, when normal impact occurs along the z axis, the stresses in the principal directions, σ_{zz}, σ_{xx}, and σ_{yy}, for the linear elastic isotropic case, are given by

$$\sigma_{zz}=\frac{E(1-\nu)}{(1+\nu)(1-2\nu)}\epsilon_{zz}, \tag{1}$$

$$\sigma_{xx}=\sigma_{yy}=\frac{\nu}{(1-\nu)}\sigma_{zz}. \tag{2}$$

The pressure is given by

$$P=\frac{(1+\nu)}{3(1-\nu)}\sigma_{zz}=K\epsilon_{zz}. \tag{3}$$

In the case of the pressure–shear experiment, an additional shear stress τ_{zx} is imposed on the above state. For shearing in the x direction, its magnitude is given by

$$\tau_{zx}=G\gamma_{xz}=2G\epsilon_{zx}=G(u_{z,x}+u_{x,z}). \tag{4}$$

Here, E, G, K, and ν are the Young's, the shear and bulk moduli, and the Poisson's ratio respectively. The ϵ are the respective strains. The shearing results in a change in the principal stress directions, depending on the shear-stress magnitude, which is usually about a quarter of the compression-pulse amplitude. The above equations are valid while the uniaxial strain condition exists. Once loading is stopped the pressure is mainly due to the in-plane stresses caused by the multiple reflections of the radial release waves and the effect of the residual shear. Since the in-plane stresses are responsible for most of the damage, a comparison of the pressure histories (or average strain), as done by Rabie and co-workers[14] and Kirkpatrick *et al.*,[15] seems to be the most meaningful approach for investigating the effects of different configurations. It considers the combined effect of the in-plane and normal stresses. Hence, this study also focuses mainly on this component, while pointing out other interesting features associated with other components.

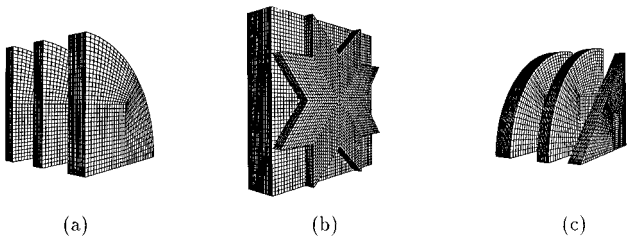

FIG. 4. Normal recovery configurations: (a) all circular plates; (b) star-shaped flyer with square plates; (c) square-shaped flyer with circular plates.

Normal recovery: The considered configurations are shown in Fig. 4. The following general features are observed from Fig. 5 for the normal recovery experiments. All quantities, i.e., the stress, pressure, and particle velocity at the midsection, exhibit an oscillating behavior about the zero value, although there is no amplification of the kind observed by Kirkpatrick*et al.*[15] Their simulation was not for a recov-

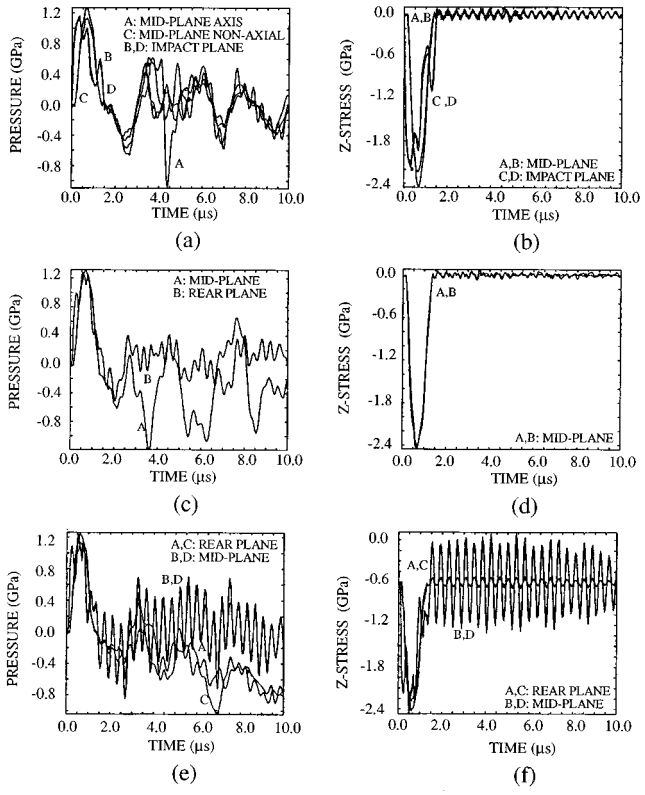

FIG. 5. Pressure and longitudinal stress histories in normal impact recovery configurations: (a),(b) all circular plates; (c),(d) star-shaped flyer—$\pi/4$ type and square plates; (e),(f) square-shaped flyer with circular plates.

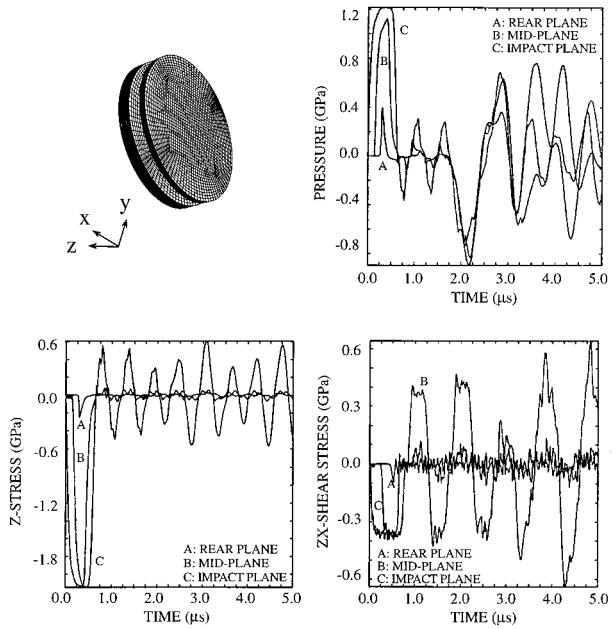

FIG. 6. Conventional pressure–shear configuration.

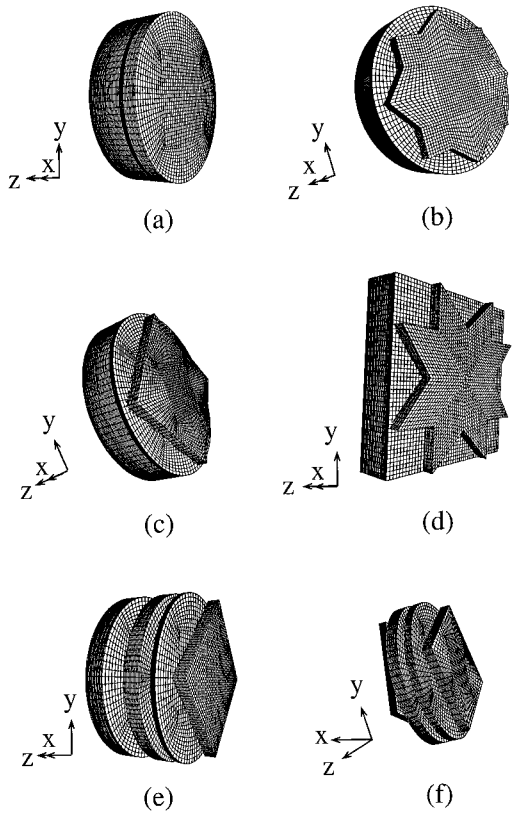

FIG. 7. Pressure–shear recovery configurations: (a) all circular plates; (b) star-shaped second flyer—$3\pi/4$ type; (c) square-shaped second flyer with circular plates; (d) star-shaped second flyer—$\pi/4$ type and square plates; (e) square-shaped flyer with critical planes on the specimen; (f) two squares—a square second flyer and a square momentum trap.

ery configuration, it did not have a momentum trap. The values at the impact and rear surfaces do not show significant oscillation. The negative pressure that occurs immediately after the unloading of the main pulse is around 50% of the main pulse amplitude in all configurations. However, after considerably longer durations, the star-shaped flyer configuration with square plates gives a better performance at locations away from the center, where the pressure becomes negative, i.e., tensile. Its magnitude is about 25% of the main pulse for the all-circular plate-type configuration and shows an increasing tendency with time, for the square-shaped configuration. It remains around 15%–20% for the star-shaped type. The release effects appear earlier in the star and square flyer configuration, because the reentrant corners of the star and the middle of the side of the square are nearer to the center. The tensile effects are worst at the center of the specimen and a sharp tensile spike appears in all configurations at 4–4.5 μs, at the rear surface, which is due to the effect that appears in σ_{xx}.

Basic pressure–shear: This simulation is for nonrecovery-type pressure–shear impact. It is carried out in order to have a simple reference configuration and to see how it differs from the normal impact simulations, carried out in the past by others. The results are as expected, and histories of some of the components are shown in Fig. 6. One feature that can be seen is that the pressure and σ_{zz} show a late-time oscillatory amplification at the center of the specimen's midsection, but are better at locations away from the center. The longitudinal release wave front from the specimen arrives at the center of the specimen at 1.8 μs, and the shear release wave front arrives at 3.2 μs. The stresses σ_{zz} and τ_{xz} go to zero at the free surfaces, while at the midsection we see a rounding and oscillating behavior for both components, as well as a late-time amplification, which could be like the mechanism of vibrations in harmonic modes referred to by Kirkpatrick *et al.*[15] The Z velocities also show that the specimen attains a mean rigid body velocity after it is separated from the target.[18]

Pressure–shear recovery: The various configurations which are simulated are shown in Fig. 7. Figures 8, 9, and 10 show the results from these simulations. A general observation valid for all these simulations is that an oscillating behavior exists at the center of the specimen's midsection, where maximum tensile stresses also occur. The mean tensile stress (negative pressure) has much lower values, at points some distance away from the midsection. One can also note that the arrival of the longitudinal release wave front does not show up clearly. This is because it reaches the center of the specimen at about the termination time of the main compression loading, and gets obscured. The arrival of the shear release wave front is the main cause for the generation of the maximum tensile stresses. For the all-circular type, the maximum tensile stress amplitude reaches the same value as the compression pulse. This event can be seen as a large reversal in amplitude for σ_{xx} at 3.2 μs.

In the case of the configuration with a star-shaped second flyer of $3\pi/4$ type, and circular plates, the amplitude of the peak tensile pulse is about 70% of the main pulse at the midsection. It is around 30% at other locations. In case of the configuration using a star-shaped second flyer of $\pi/2$ type, the tensile amplitude reaches around 55% of the main pulse

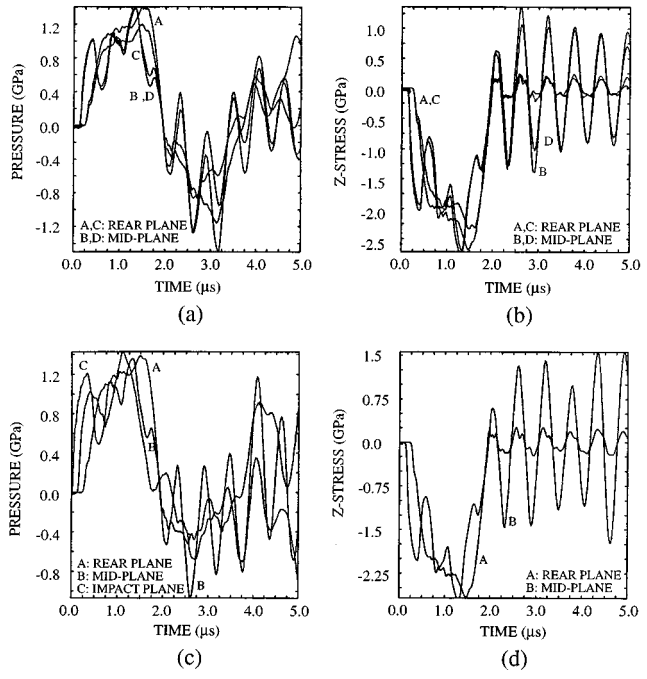

FIG. 8. Pressure–shear recovery configuration—pressure and longitudinal compression histories: (a),(b) all circular plates; (c),(d) star-shaped second flyer $3\pi/4$ type.

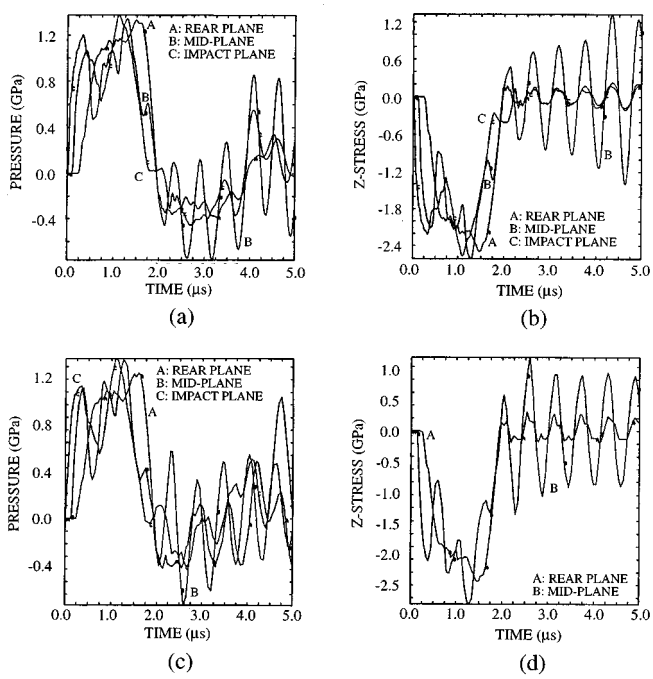

FIG. 10. Pressure–shear recovery configuration—pressure and longitudinal compression histories: (a),(b) star-shaped second flyer—$\pi/4$ type and square plates; (c),(d) square-shaped second flyer with critical planes on the circular specimen.

at the midsection, but is around 20% at the other locations. Stress σ_{zz} seems to build up at the midsection at later times.

The shear release front with the two types of star-shaped flyers discussed above appears earlier, when compared with the all-circular plates configuration, i.e., at 2.6 μs. This is because it originates at the inside corners of star flyers. For

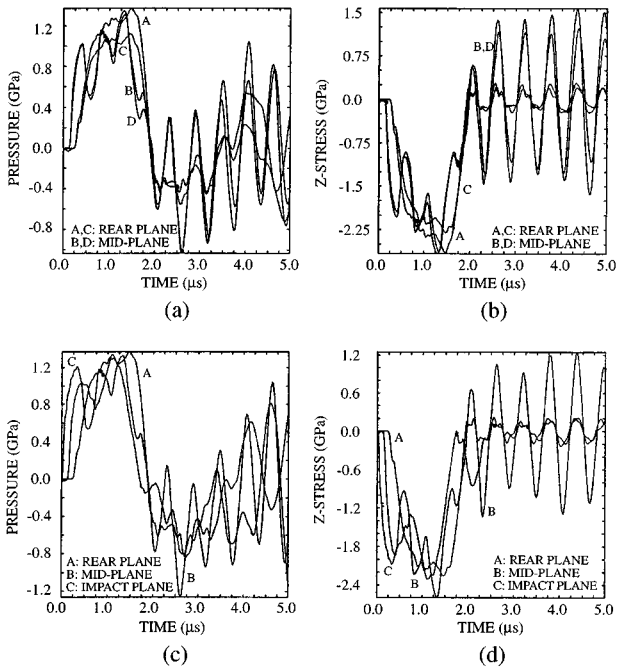

FIG. 9. Pressure–shear recovery configuration—pressure and longitudinal compression histories: (a),(b) square-shaped second flyer with circular plates; (c),(d) two squares—a second flyer and a square momentum trap.

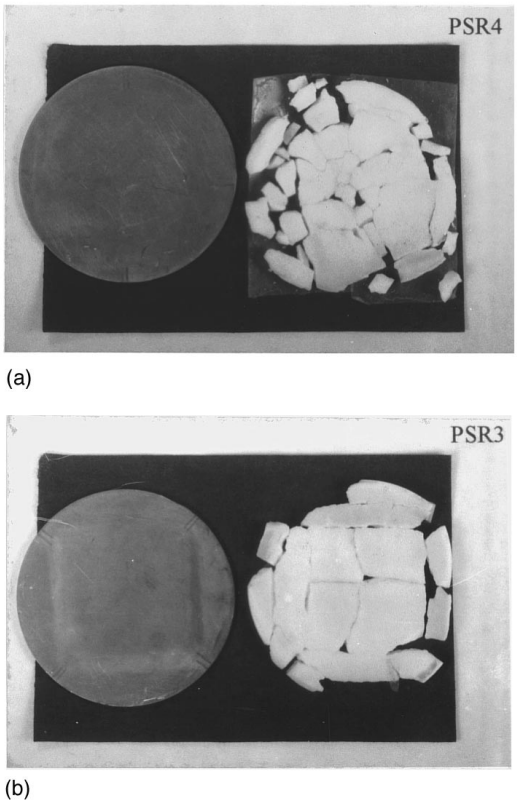

FIG. 11. Crack patterns in recovered specimens in pressure–shear recovery experiments employing (a) all circular plates and (b) a square-shaped second flyer.

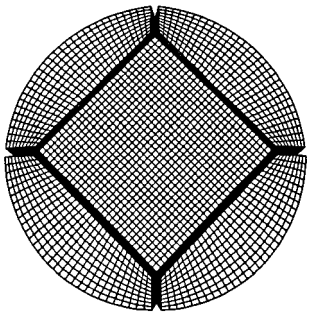

FIG. 12. Numerical simulation of the breakup with critical planes are provided.

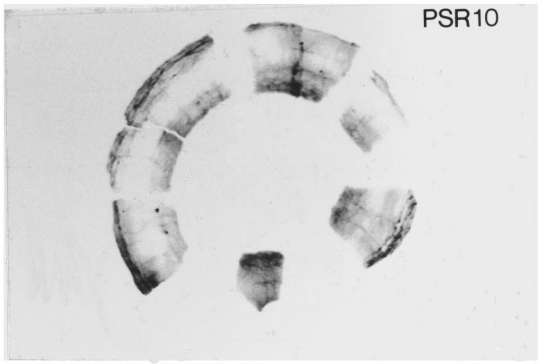

(a)

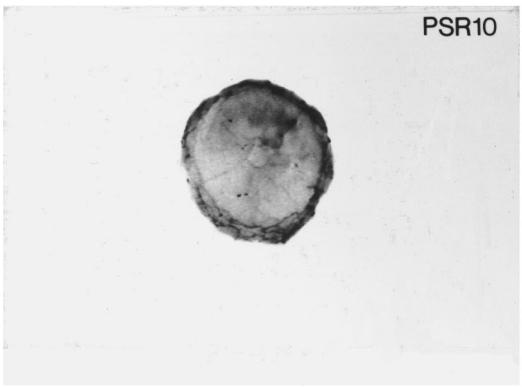

(b)

FIG. 13. (a) Outer circumferential ring and (b) the central spalled portion of the recovered specimen in a pressure–shear recovery experiment where only circular plates were used.

the configuration using a one-square flyer, the maximum tensile amplitude is around 60% and decays with time. There is very little buildup in σ_{zz}. The two-squares configuration has larger tensile mean stress amplitudes compared to the square-shaped second flyer configuration, where it first decays and then builds up. It was also observed that σ_{xx} values drift apart and stay separated at later times at the three locations along the thickness.[18] For the configuration where planes were allowed to fail at a critical tensile stress value, the maximum tensile amplitude is the least of all, around 50% of the main pulse, and it decays with time. The value in the other locations at the center also remains at the 20% level and is at the 10% level at locations away from the center. Thus, it gives a better performance compared to the other types. The simulated break up can be seen in Fig. 12.

IV. EXPERIMENTAL OBSERVATIONS AND CONCLUSIONS

Some typical results of specimen breakup, from experiments that were performed in the pressure–shear recovery and normal recovery modes, are shown in Figs. 11, 13, and 14. The experiments PSR4 and PSR10 made use of only circular plates, and experiment PSR3 was one of the one-square type. NR1 was a normal recovery experiment, with a gap at the specimen–momentum-trap interface, leading to a tensile pulse of 10–15 ns duration, similar to the one by Raiser and co-workers[11] and Sano *et al.*[19] The other details of these experiments are given in Table IV. The main features observed are that all specimens spall out a circular ring of material from the boundaries, because of the radial release and unloading wave interaction. This separation of the ring initiates flaws, resulting in favorable conditions for the macrocracks to be formed at these new boundaries. A light imprint of the fracturing specimen is captured on the first flyer, while there are no such marks on the momentum trap. The pieces of the specimen recovered afterward could be rebuilt to match perfectly with the imprint. From this, it can be concluded that the fracture of the specimen takes place after the momentum trap is separated from the specimen. This radial spalling of a ring of material from the outer boundary of the brittle ceramic specimen consumes a portion of the release energy. This aspect was not modeled. Typical results of the effect of flyer shape can be seen from experiments PSR3 and PSR4. The stress levels in these are almost identical, but the recovered specimen in PSR3 is in better shape than that of PSR4 which has broken up into several small pieces. PSR3 has only two cracks that run through its center, forming a cross shape. These cracks separate the sample into four large pieces which remain almost together after the experiment. These cracks are formed through the interaction of the cylindrical release waves which initiate at the square edges, and meet at the center of the specimen.

From the above results, it becomes clear that the cross-shaped cracks observed by Chang *et al.*,[5] in the configuration

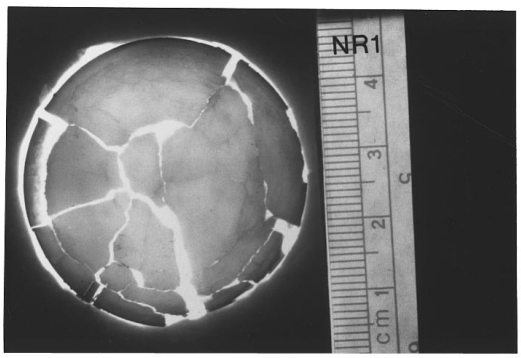

FIG. 14. Specimen recovered in the normal recovery experiment where only circular plates were used.

TABLE IV. Experimental details.

Expt. No.	Projectile velocity (m/s)	Angle (deg.)	Specimen Material	Specimen Thickness (mm)	Pressure (GPa)	Shear (MPa)	Tilt (mrad)
PSR3	80.0	23.25	AD995	3.01	1.573	386.3	0.9
PSR4	78.63	23.5	AD995	3.21	1.543	383.5	0.24
PSR10	141.1	11.26	AD995	3.03	3.896	464.4	0.08
NR1	92.36	⋯	AD995	3.24	1.98	⋯	0.22

they proposed, are also due to cylindrical release waves from the square edges of the sample. It is difficult to prevent this kind of cracking, especially when the loading durations exceed 0.5 μs. Scanning electron microscopy (SEM) observations show that the effect of these macrocracks on the material, at the microstructural level, is seen to be localized to the planes of these cracks that break up the specimen. Because of this macrocracking, the stresses seem to reduce to levels that do not affect the individual central pieces that have been formed.

Release waves are found to be the main reason for the breakup of brittle specimens in impact experiments. Here, we have examined the performance of different flyer plate geometries in several configurations which were designed to decrease the above damaging effects for recovery experiments, and have discussed their relative effectiveness for longer durations of loading. Results from simulations show that the star-shaped flyer with square plates gives a better performance for normal impact experiments at points away from the center, although we have not conducted any such normal impact experiments during this study. A square-shaped second flyer enables a redirection of energy similar to the star-shaped configuration, and allows for a controlled breakup of the specimen in the pressure–shear recovery experiments. It involves simple geometries and does not need complex machining steps. Allowing a similar breakup in normal impact simulations may also result in improved performance. The breakup in brittle materials can be predicted with high accuracy. Experimental results on aluminum oxide ceramics have substantiated the efficacy of this conclusion.

In simulations involving two-square flyers suitable modification of the thicknesses may lead to better performance. Another idea that can be pursued in this configuration is to use a square specimen instead of a circular one. The results from the simulations could also be useful for materials that are not brittle and undergo plasticity, since introduction of dissipative mechanisms such as plasticity leads to an attenuation of the tensile effects in the central region.

ACKNOWLEDGMENTS

We would like to acknowledge a helpful clarification obtained from Dr. D. J. Benson and Scott Schoenfeld regarding the use of DYNA-3D, and the support received from Chuck Charman at the San Diego Supercomputer Center (SDSC). We would also like to thank Dr. M. Beizaie for his assistance in preparing the figures in the manuscript. The computations were performed on the CRAY-90 at SDSC, and access was provided through NSF Grant No. MSS-90-21671. This research was supported by the U. S. Army Research Office under Contract No. ARO-DAAL03-86-K-0169 and No. ARO-DAAL03-92-K-0002 to UCSD.

[1] A. R. Machcha and S. Nemat-Nasser, Mech. Mater. **18**, 49 (1994).
[2] J. H. Smith, ASTM Tech. Pub. **336**, 264 (1963).
[3] W. F. Hartman, J. Appl. Phys. **35**, 2090 (1964).
[4] S. N. Chang, D. T. Chung, G. Ravichandran, and S. Nemat-Nasser, in *Shock Compression of Condensed Matter*, edited by S. C. Schmidt and L. W. Davidson (1989), p. 389.
[5] S. N. Chang, D. T. Chung, Y. F. Li, and S. Nemat-Nasser, J. Appl. Mech. Trans. ASME **59**, 305 (1992).
[6] L. H. L. Louro and M. A. Meyers, in *Shock Compression of Condensed Matter*, edited by S. C. Schmidt, J. N. Johnson, and L. W. Davidson (1989), p. 465.
[7] P. Kumar and R. J. Clifton, J. Appl. Phys. **48**, 4850 (1977).
[8] J. E. Vorthman and G. E. Duvall, J. Appl. Phys. **53**, 3607 (1982).
[9] F. Longy and J. Cagnoux, in *Shock Compression of Condensed Matter*, edited by S. C. Schmidt, J. N. Johnson, and L. W. Davison, p. 441.
[10] D. Yaziv, Ph. D. thesis University of Dayton, 1985.
[11] G. Raiser, R. J. Clifton, and M. Ortiz, Mech. Mater. **10**, 43 (1990).
[12] H. D. Espinosa, G. Raiser, R. J. Clifton, and M. Ortiz, J. Appl. Phys. **72**, 3451 (1992).
[13] A. L. Stevens and O. E. Jones, J. Appl. Mech. Trans. ASME **30**, 359 (1972).
[14] R. L. Rabie, J. E. Vorthman, and J. K. Dienes, in *Shock Waves in Condensed Matter*, edited by J. R. Asay, R. A. Graham, and G. K. Straub (1983), p. 199.
[15] S. W. Kirkpatrick, D. R. Curran, D. C. Erlich, and R. W. Klopp, in *Shock Compression of Condensed Matter*, edited by S. C. Schmidt, R. D. Dick, J. W. Forbes, and D. G. Tasker (1991), p. 935.
[16] A. R. Machcha and S. Nemat-Nasser, presented in part at the 12th U. S. National Congress of Applied Mechanics held at Seattle Session 3CA7, Dynamics Behavior of Advanced Materials I, June 27–July 1, 1994.
[17] J. O. Hallquist and D. J. Benson, Report No. UCID 19592, Rev. 2, Lawrence Livermore National Laboratory, 1986.
[18] A. R. Machcha, Ph.D. thesis, University of California, San Diego, 1994.
[19] Y. Sano, S. N. Chang, M. A. Meyers, and S. Nemat-Nasser, Acta Metall. Mater. **40**, 413 (1992).